THE JOURNAL OF PHYSICAL CHEMISTRY A
A JOURNAL OF THE AMERICAN CHEMICAL SOCIETY

pubs.acs.org/JPCA Article

Anisotropy Measurements from the Near-Threshold Photodissociation of the N_2−NO Complex

Bradley F. Parsons,* Adrian W. Draney, Hunter J. Warder, Marcos R. Rivera, and Michael K. Onder

Cite This: https://doi.org/10.1021/acs.jpca.1c10514 Read Online

ACCESS | Metrics & More | Article Recommendations | Supporting Information

ABSTRACT: We have used velocity map ion imaging to measure the angular anisotropy of the NO (A) products from the photodissociation of the N_2−NO complex. Our experiment ranged from 108 to 758 cm^{-1} above the threshold energy to form NO (A) + N_2 (X) products, and these measurements reveal, for the first time, a strong angular anisotropy from photodissociation. At 108 cm^{-1} above the photodissociation threshold, we observed NO (A) photoproducts recoil preferentially perpendicular to the laser polarization axis with an average anisotropy parameter, β = −0.25; however, as the available energy was increased, the anisotropy increased, and at 758 cm^{-1} above the threshold energy, we found an average β = +0.28. The observed changes in the angular anisotropy of the NO (A) photoproduct are qualitatively similar to those observed for the photodissociation of the Ar−NO complex and likely result from changes in the region of the excited state potential energy surface accessed during the electronic excitation. At the lowest available energy, we also noted a large contribution from hotband excitation; however, this contribution decreased as the available energy increased. The outsized contribution at the lowest available energy may result from hotbands having better Franck−Condon overlap with the excited electronic state near threshold. Finally, we contrast the experimental center of mass translational energy distribution with a statistical energy distribution determined from phase space theory. The experimental and statistical distributions show pronounced disagreement, particularly at low kinetic energies, with the experimental one showing less dissociation resulting in high rotational levels of the fragments.

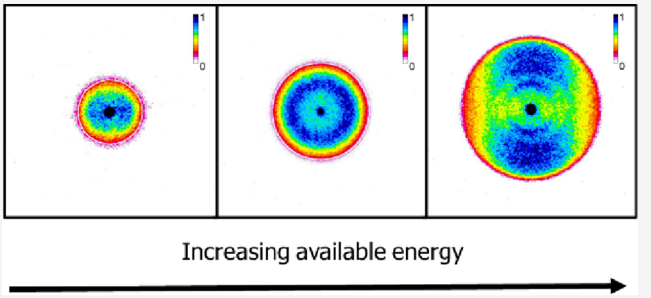

1. INTRODUCTION

Laser-induced fluorescence (LIF) is an important tool in measuring atmospheric NO concentrations and can allow for a subpart per trillion determination of this pollutant.[1] During LIF measurements, ground state NO ($X\ ^2\Pi$) is promoted to the lowest excited state NO ($A\ ^2\Sigma+$) and the fluorescence signal is monitored.[1] However, quenching of NO (A) by small gas-phase species can reduce the measured LIF signal. As an example of a simple closed-shell molecule paired with open-shell nitric oxide, the N_2−NO collision complex can serve as a benchmark to further our understanding of the quenching of excited NO (A). The quenching rate constant for N_2 and NO (A) is known,[2] and recent work has improved our understanding of the N_2−NO (A) excited state that ultimately results in electronic quenching.[3−5] In particular, a very recently published potential energy surface found the N_2−NO (A) excited state to have a conical intersection that may funnel population to the ground state of the complex, leading to quenching.[3]

The ground state for the N_2−NO complex has been extensively studied using both electronic structure calculations and experiments.[4,6−10] The overall results for the ground state are consistent with relatively low barriers to internal rotation for the diatomic moieties, resulting in a floppy complex having a minimum geometry with the NO bond approximately perpendicular to the Jacobi vector between the NO center of mass (CM) and N_2 CM.[9,10] We henceforth refer to this complex geometry as T-shaped. For the excited state, Lozeille et al. performed electronic structure calculations and found nonlinear geometries reverted to the ground state, so only linear excited state geometries were discussed.[4] They considered both NO··N_2 and ON··N_2 linear isomers and found the latter to be more stable, with a predicted binding energy of 230 cm^{-1} from their RCCSD(T)/aug-cc-pVTZ calculation.[4] More recently, Luxford et al. investigated NO (A) and N_2 using crossed molecular beam scattering coupled with velocity map ion imaging (VMI).[5] In their experiment, the differential cross section for NO (A) showed an extremely forward-scattered peak, which was similar to that observed for the NO (A) + Ar system.[11] The observed feature in NO (A) +

Received: December 13, 2021
Revised: February 7, 2022

Ar resulted from a well on the excited potential near the N atom side, and so they postulated that NO (A) + N_2 also has a well near the N atom side of NO, which was consistent with the calculations of Lozeille et al.[4,5] Very recently, Guardado et al. published potential energy curves for the ground and lowest excited states of N_2−NO.[3] They used a variant of the equation-of-motion coupled-cluster singles and doubles method, EOM-EA-CCSD/aug-cc-pVDZ, to perform constrained optimizations and then determine the energy from a single point calculation with a larger basis set, EOM-EA-CCSD/d-aug-cc-pVTZ.[3] The N_2 moiety splits the degenerate NO (X $^2\Pi$) ground state potential energy surface into a pair of states labeled as D_0 (X $^2\Pi$ A″) and D_1 (X $^2\Pi$ A′).[3] In their calculation they located a conical intersection between the D_1 state and the excited D_2 (A $^2\Pi$ A′) state, which is accessed during the transition. They also found an angle-dependent barrier in the range of 0.2 eV, which is due to an avoided crossing between the D_2 state and the higher energy D_4 (C $^2\Pi$ A′) state. The barrier separates the conical intersection of the D_1 and D_2 states from the region of the excited state readily accessed during a vertical electronic transition from the minimum N_2−NO ground state geometry.[3] We also note that while the conical intersection may funnel population from the D_2 excited state to the D_1 state, it is not accessible at the energies in our current experiments due to the barrier. Finally, Guardado et al. found that the minimum energy geometry for the (A $^2\Sigma^+$A′) excited state is linear with an R_{NN} of 3.19 Å and a binding energy of 335.02 cm^{-1}.[3]

The recent publication of an excited state potential energy surface for N_2−NO has prompted our reinvestigation of the complex. Based on the potential energy surfaces, N_2−NO shares features in common with the Ar−NO complex, for which the ground state is also T-shaped[12] and the lowest excited state is also linear.[13,14] Holmes-Ross et al. undertook extensive experimental and theoretical studies of the Rg−NO complexes (Rg = He, Ne, and Ar).[13,15−17] In their final work, Rg−NO was photodissociated and the NO (A) products were detected using state-selective ionization coupled with VMI.[13] The experimental NO (A) rotational state distributions were compared with the results of time-dependent wavepacket calculations using the ground and excited state potential energy surfaces, and the results showed good agreement between theory and experiment.[13] In addition, they observed pronounced changes in the NO (A) photoproduct angular distribution as a function of excitation energy. Holmes-Ross et al. began their analysis of the experimental NO (A) angular distribution by noting that for direct (prompt) dissociation, the angular distribution, $I(\theta)$, may be described by the equation[13,18]

$$I(\theta) = \frac{1}{4\pi}[1 + \beta P_2(\cos\theta)] \quad (1)$$

where $P_2(\cos\theta)$ is the second Legendre polynomial and β is the anisotropy parameter, which ranges from −1 for photofragments recoiling perpendicular to the laser polarization axis to +2 for fragments recoiling parallel to the polarization axis. At low excitation energies, Holmes-Ross et al. observed NO (A) fragments with $\beta < 0$, which was consistent with the previous near-threshold measurements by Roeterdink et al.[13,19] Moreover, Holmes-Ross et al. observed that β increased and became positive as the excitation energy increased.[13] To explain the observed trend for β versus available energy, they note that for Rg−NO, the transition dipole is fixed to the NO moiety and perpendicular to the NO bond. Furthermore, they note that the floppy Ar−NO complex can undergo large amplitude motions; however, they qualitatively explain the observed β values by arguing that for a well-defined complex geometry, dissociation of a linear Ar−NO complex will result in $\beta = -1$. They also note that T-shape complexes may result in $\beta = +2$ or $\beta = -1$, which gives an averaged value of $\beta = +0.5$.[13] In Figure S1 of the Supporting Information, we provide a cartoon of the laboratory frame orientations for linear and T-shape X−NO complexes resulting in these limiting β values. Using the available potential energy surfaces, Holmes-Ross et al. found that excitation at 100 cm^{-1} above the threshold should access the excited state near $\gamma = 50°$, where γ is the Jacobi angle between the NO bond and the vector **R**, between the NO CM and the Ar atom.[13] Alternatively, they find excitation at 400 cm^{-1} above the threshold to be most heavily weighted near $\gamma = 90°$.[13] Thus, the qualitative differences in β result from different regions of the excited state potential energy surface being accessed, whereby excitation far above the threshold accesses a region more closely resembling the T-shape ground state, while excitation close to the threshold accesses a region further removed from the ground state minimum geometry.

In this work, we measure the NO (A) recoil anisotropy for the photodissociation of N_2−NO using VMI from about 108 to 758 cm^{-1} above the threshold to form NO (A) + N_2 (X) products. In Section 2, we briefly explain our setup for these experiments including modifications to reveal wavelength-dependent anisotropy changes. In Section 3, we present the experimental results and the kinetic energy distribution from phase space theory (PST). In Section 4, we compare our experimental β values with previous observations for Ar−NO. We also discuss the contribution of hotbands in near-threshold excitation and contrast the experimental CM kinetic energy distributions with those from PST. Finally, we discuss planned future experiments and then present a brief conclusion in Section 5.

2. EXPERIMENTAL SECTION

The VMI apparatus used for these experiments has been described previously.[10,20] For this experiment, we prepared a gas mixture of 0.5% NO (Matheson), 9% N_2 (Matheson), and ∼90.5% He (Matheson) in a sample cylinder. The gas is introduced into the source region of the vacuum chamber through a solenoid nozzle (General Valve, 0.5 mm orifice). In the experiment, we used a nozzle backing pressure of ∼1 atm, resulting in a supersonic expansion leading to the formation of the N_2−NO complex. The supersonic expansion passes through a skimmer, resulting in a molecular beam that enters the main chamber of our apparatus, which houses conventional VMI optics.[21] For the experiment, the first and second plates of the four-plate ion optic stack are held at +500 and +360 V, respectively, and the final two plates are grounded, which results in an NO^+ flight time of 12.9 μs. The ion flight time, along with the magnification factor or instrument function, is used for subsequent determination of the NO speed. We have included a discussion for the calibration of the magnification factor in the Supporting Information.

We generate laser light using an Nd:YAG-pumped dye laser (Spectra Physics LAB-190-10H, 10 ns pulse, Sirah Cobra Stretch, 0.24 cm^{-1} UV bandwidth), which we operate using Coumarin 450 laser dye (Exciton/Luxottica) dissolved in ethanol (200 proof, Fischer Scientific). We generate laser photons between 222 and 225.26 nm by frequency doubling

https://doi.org/10.1021/acs.jpca.1c10514
J. Phys. Chem. A XXXX, XXX, XXX−XXX

the dye laser output using a β barium borate crystal. The ultraviolet (UV) laser beam has a diameter of about 1 cm and is focused onto the molecular beam with a 500 mm lens. UV photons dissociate the complex into N_2 and NO (A) products, and the latter are nonresonantly ionized following the absorption of a second photon. We project the resulting cations onto a two-dimensional position sensitive detector (Sydor Technology) and record images using a charge-coupled device (CCD) camera (QCam Fast 1394).

To detect the NO (A) recoil anisotropy, we have made several changes to our experiment. We use a 12-bit CCD camera to record individual images, so each pixel corresponds to 2^{12} = 4096 counts; however, individual ions result in ~2000 counts at the center pixel. Thus, for an individual image, more than two ions per pixel leads to saturation. For this experiment, we eliminate the contribution from two ion events in individual images by reducing the NO^+ ion levels per laser shot, which also minimizes space charge effects. Previously, we reduced NO^+ ion levels by varying the Nd:YAG pump laser power and by using an iris to eliminate part of the UV laser beam. However, for these experiments, we instead dynamically reduce the UV laser output power using a variable $\lambda/2$ waveplate (ALPHALAS GmbH) and a Glan laser polarizer (ThorLabs) set to pass vertically polarized light. This setup allows for careful control over the laser power levels, resulting in about 100−200 μJ per pulse, which in turn reduces observed NO^+ ion levels and eliminates two ion events resulting in image saturation. The individual ion images typically correspond to a 10 s exposure time and have very few ions (~1 or 2 ions per laser shot), which results in low signal-to-noise. Thus, we use the ImageJ program[22] to rapidly sum many individual images, typically ~360, to create a high signal-to-noise composite image for subsequent analysis.

3. RESULTS

We first confirmed the formation of the N_2−NO complex by recording the mass spectrum of the molecular beam. The molecular beam contents were ionized near 225 nm, and the ions were projected onto the detector. We recorded the ion signal as a function of flight time using a digital storage oscilloscope (Tektronix TDS 2024C). The resulting mass spectrum was calibrated with the measured flight time for H^+, C^+, and NO^+, which were observed from the cracking of hydrocarbon vacuum pump oil and uncomplexed NO. Figure 1 shows the resulting mass spectrum of the molecular beam versus the fragment mass from m/z = 20 to 90.

In Figure 1, the most intense signal is observed at m/z = 30, corresponding to uncomplexed NO in the molecular beam. Figure 1 shows a small signal at m/z = 58, which varied with valve backing pressure and timing. The signal at m/z = 58 corresponds to N_2−NO and an expanded view is shown in the inset. We observed no ion signal at either m/z = 86 or 88, which would correspond to the $(N_2)_2$−NO or N_2−$(NO)_2$ ions, respectively, so the molecular beam consisted of uncomplexed NO with a small population of the bimolecular N_2−NO complex and the latter was optimized using valve timing. We also attempted to measure the NO^+ ion signal from N_2−NO photodissociation as a function of the excitation laser wavelength, similar to Roeterdink et al., who used a two-laser pump probe experiment to observe several transitions to the Ar−NO excited state, which were attributed to Feshbach resonances.[19] However, for N_2−NO, we were unable to observe any wavelength-dependent signal different from that due to uncomplexed NO (X) using our one laser experiment.

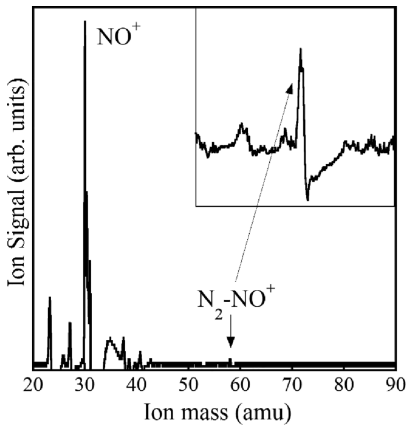

Figure 1. Mass spectrum of the molecular beam between m/z = 20 and 90. The inset shows the signal at 58 amu, corresponding to N_2−NO^+.

We next photodissociate the N_2−NO complex and record the NO^+ velocity map ion images as a function of available energy, E_{avail}, which is given by eq 2

$$E_{avail} = E_{photon} + E_{int,complex} - D_0'' - \nu_{00,NO} - E_{rot,NO} - E_{rot,N_2} \quad (2)$$

where the term energy, $\nu_{00,NO}$, for the NO (A) ← NO (X) transition is taken from Tsuji et al. to be 44 198.9 cm^{-1}.[23] Our laboratory previously measured the NO (A) threshold energy from N_2−NO to be 44 284.7 cm^{-1}, which gave the complex ground state dissociation energy, D_0'', to be 86 cm^{-1}.[10] The internal energy of the complex before excitation is given by $E_{int,complex}$ and the rotational energy for the NO or N_2 fragments following dissociation is as follows: $E_{rot,NO}$ and $E_{rot,N2}$, respectively. For all the experiments, we calculate the available energy, assuming no internal energy of the complex, and then indicate that the portion of the experimental data that extends beyond E_{avail}.

In Figure 2, we present two NO^+ velocity map ion images following the photodissociation of the complex. The lower ion image in Figure 2A results from excitation at 225.26 nm, which corresponds to 108 cm^{-1} of available energy, and the upper image in Figure 2B is for excitation at 222.00 nm, which corresponds to 758 cm^{-1} of available energy. The NO^+ ion images for all other wavelengths in this study are given in Figures S2 through S7 of the Supporting Information. In each ion image, we have also superimposed a white circle at the maximum radius corresponding to the available energy; thus, all NO^+ beyond the inner edge of this circle has some internal energy before excitation and therefore originates from hotbands.

The vertical arrow in Figure 2A gives the laser polarization direction used during our experiment. We transform the observed ion images using both the pBasex method[24] and the BaseX program[25] to determine the NO (A) velocity distribution and recoil anisotropy. As discussed in the Supporting Information, the resulting NO (A) velocity distribution is transformed into a CM kinetic energy distribution. In Figure 3, we show the resulting CM kinetic energy distributions, $P(E_T)$, corresponding to the ion images given in Figure 2. The $P(E_T)$ shown in Figure 3 (bottom)

https://doi.org/10.1021/acs.jpca.1c10514
J. Phys. Chem. A XXXX, XXX, XXX−XXX

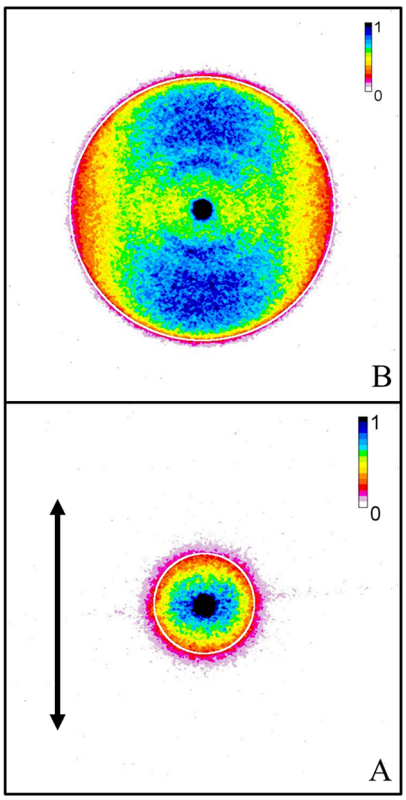

Figure 2. NO^+ ion images showing the observed recoil anisotropy. The lower image (A) was obtained with E_{avail} = 108 cm^{-1} energy, while the upper image (B) was obtained with E_{avail} = 758 cm^{-1}. The vertical arrow in the lower frame gives the orientation of the laser polarization. A calibration bar for the color map is given in the upper right corner of the ion images, and the blue and black regions correspond to high ion intensity, while the yellow, orange, and red regions correspond to low ion intensity. A white circle is superimposed on the ion image at the maximum radius corresponding to NO fragments recoiling from dissociation with CM translational energy equal to E_{avail}, and all the NO fragments beyond the inner edge of the white circle must have some energetic contribution from hotbands.

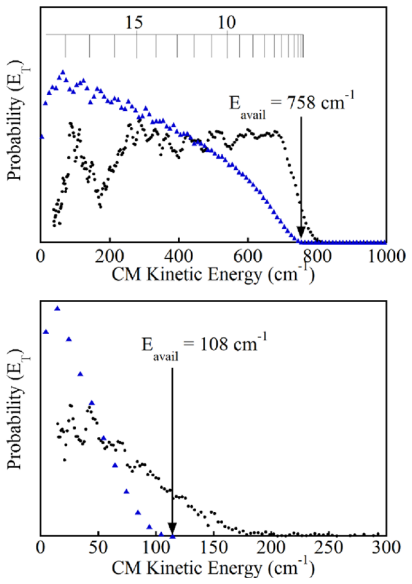

Figure 3. CM kinetic energy distributions for photodissociation at E_{avail} = 758 cm^{-1} (top) and E_{avail} = 108 cm^{-1} (bottom). The black points are the experimental data, and the blue triangles are the CM kinetic energy distribution from PST. The comb at the top of the upper frame corresponds to the CM kinetic energy expected following dissociation with either diatomic fragment formed in an excited rotational level.

corresponds to 108 cm^{-1} of available energy and the $P(E_T)$ in Figure 3 (top) corresponds to 758 cm^{-1} of available energy. The vertical arrows in Figure 3 indicate the maximum available energy for excitation from a complex with zero internal energy. The CM kinetic energy distributions at all other energies are given in Figures S2 through S7 of the Supporting Information.

At the wavelengths used in this study, the photodissociation of the N_2−NO complex may result in both N_2 (X) and NO (A) formed in several excited rotational levels, but neither fragment may be formed in a vibrationally excited state. Thus, we contrast the experimental data with that expected for a completely statistical dissociation using PST.[26−29] Because we are currently limited to a one laser experiment with nonresonant ionization of all the NO (A) products, we cannot separately determine the rotational state distribution for either fragment. Thus, as discussed in the Supporting Information, we find the probability of forming each pair of allowed N_2 and NO (A) rotational states using the PST state counts based on the conservation of energy and angular momentum.[27−29] We then determine the corresponding translational energy for each pair of states and bin the probabilities as a function of energy. The resulting PST kinetic energy distributions are given by the blue triangles in Figures 3 and S2 through S7 of the Supporting Information.

4. DISCUSSION

The principal goal of this study was to investigate changes in the recoil anisotropy for the NO (A) fragment as a function of E_{avail}. Although the NO^+ images in our original study did not show any recoil anisotropy[10] because of modifications to the experiment, we now observe significant recoil anisotropy in the ion images, Figures 2 and S2 through S7. Referring to the maximum NO^+ ion intensity given by the blue regions in Figures 2A and S2 and S3, NO fragments are observed to have a more perpendicular angular distribution, $\beta < 0$, at low available energies. At high available energies, Figures 2B and S6 and S7, the maximum NO^+ intensity in the ion images (blue regions) appears with a more parallel angular distribution with $\beta > 0$. We note that very similar behavior was also observed for the photodissociation of Ar−NO where the general trend was illustrated by plotting the anisotropy parameter, β, for the lowest rotational level of NO (A) versus available energy.[13] Because our current experiment does not use state-selective ionization of NO, our ion images contain overlapping contributions from the energetically allowed combinations of NO (A) and N_2 (X) rotational levels, and thus we cannot unambiguously extract the contribution resulting from NO (A) formed in a particular rotational state. Hence, we instead find the NO recoil anisotropy parameter, obtained using the BaseX program,[25] within ∼±5−10 cm^{-1} of the *average* energy determined from the experimental $P(E_T)$ for each E_{avail} in this study. The results are plotted in Figure 4 and illustrate the general trend of $\beta < 0$ at low E_{avail} but with $\beta > 0$ at high E_{avail}. In Table S1 of the Supporting Information, we give the β values from Figure 4 along with β values obtained by averaging the anisotropy parameter over the central energy range for each $P(E_T)$, and both methods give similar results. Finally, in

https://doi.org/10.1021/acs.jpca.1c10514
J. Phys. Chem. A XXXX, XXX, XXX−XXX

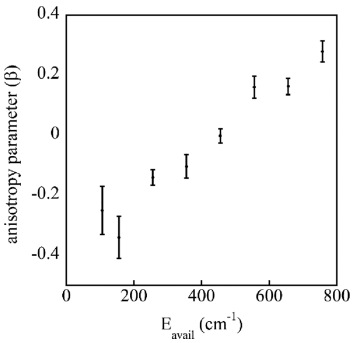

Figure 4. NO (A) recoil anisotropy parameter for the photodissociation of the N_2−NO complex versus available energy.

Figures S8 through S15 of the Supporting Information, we give the experimentally observed β as a function of CM translational energy for each E_{avail} in this study.

Figure 4 shows a similar trend for β versus E_{avail} as that observed for Ar−NO photodissociation.[13] As discussed in the Introduction, for Ar−NO, Holmes-Ross et al. argued that far above the threshold, an electronic transition from the T-shape ground state of Ar−NO accesses the excited state potential energy surface with a Jacobi angle γ near 90° (corresponding to a T-shape like geometry) and prompt photodissociation from this region of the excited state would then result in $\beta > 0$. For N_2−NO at high E_{avail}, we also expect electronic excitation from the T-shape ground state[9] to access a qualitatively similar region of the excited state and prompt dissociation may then result in $\beta > 0$, which is consistent with the experimental observations in Figure 4.

Alternatively, for photodissociation at low available energies, the delocalized ground state wavefunction for the floppy Ar−NO complex results in electronic excitation to a region of the excited state weighted near a Jacobi angle γ of 50°.[13] Prompt photodissociation of the Ar−NO complex from this region of the excited state would then result in $\beta < 0$, which was consistent with the experimental observation.[13] Likewise, for N_2−NO, the ground state potential energy surface is shallow, which should result in a delocalized ground state wavefunction. Thus, electronic excitation at low available energies may access a different region of the excited state with a smaller Jacobi angle between the NO bond and the vector between the NO and N_2 CMs. Prompt photodissociation from this region of the excited state may then result in the observed negative anisotropy parameters for E_{avail} below 260 cm^{-1} in Figure 4. Thus, as for Ar−NO, the observed changes in β versus E_{avail}, shown in Figure 4, likely result from changes in the region of the excited state accessed during the electronic transition.

We next consider the CM recoil kinetic energy distributions, $P(E_T)$ given in Figures 3 and S2 through S7 of the Supporting Information. We first examine the contribution of hotbands in the experimental $P(E_T)$. In Figures 3 and S2 through S7, the vertical arrow indicates the maximum CM translational energy corresponding to the available energy. In all the cases, the experimental $P(E_T)$ extends beyond E_{avail} and by taking the difference between the high energy tail of the experimental $P(E_T)$ and the available energy, we estimate the maximum internal energy in hotbands of the complex to be about 80 ± 10 cm^{-1} averaged over all the E_{avail} studied here. This hotband energy, obtained from the high energy tail of the experimental $P(E_T)$, is close to the ground state dissociation energy from our previous work, 86 cm^{-1}.[10] Similar high energy tails were also observed for the photodissociation of Ar−NO, with the high energy tail extending as much as 100−110 cm^{-1} beyond the available energy, compared with a complex dissociation energy of 88 cm^{-1}.[17] Furthermore, for excitation at 50 cm^{-1} of available energy, the contribution from vibrationally excited Ar−NO was estimated to be as much as 60% of the total contribution from the ground vibrational state.[17] For N_2−NO, we can likewise estimate the minimum contribution from hotbands using the experimental $P(E_T)$. At 108 cm^{-1} of available energy, Figure 3 bottom, the area of the normalized $P(E_T)$ beyond the available energy is 0.17, giving a 17% hotband contribution, which is a lower bound since hotbands may also contribute *below* E_{avail}. We observe the minimum hotband contribution decreases as available energy increases, with hotbands contributing about 8.5% at E_{avail} of 158 cm^{-1} and decreasing to about 1% at the highest available energies. We can compare the hotband contribution at the lowest E_{avail} of 108 cm^{-1} with that reported for Ar−NO.[17] For the comparison, we normalize the minimum N_2−NO hotband contribution, 0.17, with the maximum contribution from the ground vibrational state, 0.83. Thus, at the lowest available energy for N_2−NO, hotband excitation corresponds to at least 20% of the total contribution from the ground state. Although this is about one-third of the hotband contribution observed for Ar−NO, 60%, the measurement for Ar−NO was at a lower available energy (50 cm^{-1}).[17] Thus, for both complexes hotbands make a significant contribution to the near-threshold excitation. For Ar−NO, the outsized hotband contribution to near-threshold excitation was attributed to better the Franck−Condon overlap for excited vibrational levels of the approximately T-shaped ground state to the linear Ar−NO excited state.[17] A similar mechanism may account for the enhanced contribution of hotbands near threshold when exciting from a T-shaped N_2−NO ground state to a linear excited state; however, a better understanding of hotbands requires state-selective experiments detailed at the end of this section.

We previously found the average translational energy from the observed kinetic energy distributions was consistent with a simple non-statistical impulsive model.[10] For an impulsive dissociation, we expect a non-statistical $P(E_T)$ and so we now contrast the experimental $P(E_T)$ with a statistical distribution from PST.[27−29] The blue triangles in Figures 3 and S2 through S7 correspond with the PST kinetic energy distribution assuming dissociation of a complex with zero internal energy. As expected, the PST distribution does not reproduce the experimental $P(E_T)$ and as excitation energy increases, the PST distribution peaks at low CM translational energies, which is in sharp contrast with the experimental $P(E_T)$. As an example, for 659 cm^{-1} of available energy, Figure S7, we find the experimental $P(E_T)$ decreases to near zero for translational energies below ~250 cm^{-1}, which results from a hole toward the center of the ion image. No background subtraction was performed, so this is not an experimental artifact. We also observe similar behavior at 358, 458, 558, and 758 cm^{-1} above the threshold, Figures S4−S6 and 3 (top), which indicates the highest energetically allowed rotational states are less populated compared with the statistical prediction. We note that for the photodissociation of Ar−NO at available energies above ~350 cm^{-1}, the highest energetically allowed rotational levels show low or zero populations.[13,30] For Rg−NO complexes, Holmes-Ross et al. compared the NO (A) rotational state distribution as a function of E_{avail} with time-

https://doi.org/10.1021/acs.jpca.1c10514
J. Phys. Chem. A XXXX, XXX, XXX−XXX

dependent wavepacket calculations and found the observed distribution resulted from an anisotropy of the excited state potential along the NO bending coordinate.[13] For N_2−NO, we note again that Guardado et al.'s recent potential energy surface shows a significant angle-dependent barrier on the D_2 ($A\ ^2\Sigma^+$) excited state that is accessed during the electronic transition.[3] The barrier results in an excited state anisotropy, and so, as with Ar−NO,[13] an angular anisotropy of the N_2−NO excited state may contribute to a non-statistical dissociation, leading to the observed experimental $P(E_T)$.

Next, we note that at 758 cm^{-1} of available energy, Figure 3 (top), we observed a partially resolved band at low kinetic energy, which is also not consistent with the PST distribution. This band has an average translational energy of 129 cm^{-1}, which corresponds to 629 cm^{-1} of internal energy distributed between the NO (A) and N_2 (X) fragments. We consider three possible origins for this band. First, we consider electronic quenching since, as mentioned previously, the recently published excited state potential energy surface found a conical intersection, leading to electronic quenching of NO (A) products. In Figure 3 (top), the available energy, 758 cm^{-1}, is not high enough to overcome the barrier to the conical intersection, leading to electronic quenching.[3] Moreover, from the NO (A) term energy, 44 198.9 cm^{-1},[23] we expect electronic quenching would partition more than 129 cm^{-1} into CM translational energy, making quenching an unlikely origin for the band. Second, the 1 ← 0 vibrational transition corresponds to 2354 cm^{-1} of energy for NO (A) and 2330 cm^{-1} for N_2 (X).[31] Thus, we also eliminate vibrational excitation as a result in the observed band, which corresponds to only 629 cm^{-1} of internal energy. Finally, both NO (A) and N_2 (X) have nearly identical rotational constants ∼1.99 cm^{-1},[31] and we cannot resolve the NO (A) parity levels for a band with a full width at half maximum of 49 cm^{-1}. The comb in the top frame of Figure 3 indicates the expected CM translational energy corresponding to the rotational excitation of a diatomic fragment with a rotational constant of 2 cm^{-1}. A comparison with the observed band shows that energetically, this may indeed be consistent with several rotational levels; however, we cannot confidently assign the band to a particular set of level(s) without the planned experiments discussed in the next paragraph.

The current experiments lack state-selective ionization, which prevented the determination of rotational levels of either NO (A) or N_2 (X). As mentioned already, each NO (A, n) rotational state is correlated with a N_2 (X) rotational state distribution, and these correlated distributions overlap and cannot be unambiguously extracted from our experimental $P(E_T)$. Although our laboratory is currently limited to one laser experiments, we are now working to restore a second dye laser (Spectra Physics PDL-3) for use in future two-laser pump probe experiments. In the planned experiments, a pump photon from our current dye laser accesses the N_2−NO (A) excited state between 220 and 225.5 nm while the second dye laser state-selectively probes the NO (A) photoproduct near 600 nm using the known E ← A NO resonance-enhanced multiphoton ionization (REMPI) transitions similar to previous work with the Ar−NO complex.[13,15,16,19,30] This experiment allows for the observation of the complete NO (A) rotational state distribution through REMPI spectroscopy. Furthermore, detection of specific NO (A, n) levels using VMI is then used to determine the correlated N_2 rotational states. Ideally, the correlated rotational state distributions may then be compared with theoretical models using the recent excited state potential[3] and the ground state potential,[9] as was done for the Rg−NO complexes.[13] Moreover, state-selective ionization of NO (A) also eliminates the background from uncomplexed NO (X) and allows for a more precise measurement of the NO (A) threshold energy and an exploration of the hotband contribution in the experiment.

5. CONCLUSIONS

The primary goal of this work was to observe the anisotropy in the NO (A) recoil angular distribution following the photodissociation of the N_2−NO complex. We photodissociated the complex at E_{avail} ranging from 108 to 758 cm^{-1} and nonresonantly ionized the resulting NO (A) photoproducts and recorded the NO^+ velocity map ion images. These images reveal, for the first time, a pronounced anisotropy in the NO (A) product angular distribution. We compared the observed trend in β versus E_{avail} with previous results for the Ar−NO complex.[13] As with Ar−NO, an electronic transition from the floppy T-shape N_2−NO ground state accesses different regions of the nominally linear excited state as the excitation energy increases, and photodissociation from the different regions likely results in the observed trend in β. We also observed that at the lowest available energy, hotband excitation accounts for at least 17% of the observed photofragments, and the experimental $P(E_T)$ is non-statistical. Finally, we outline planned future experiments to better understand the dynamics of the N_2−NO complex.

■ ASSOCIATED CONTENT

Supporting Information

The Supporting Information is available free of charge at https://pubs.acs.org/doi/10.1021/acs.jpca.1c10514.

Discussion of instrument calibration, discussion of transformation from velocity to CM translational energy, discussion of PST distribution, cartoon showing laboratory frame orientations of X−NO complex with limiting β values, velocity map ion images and CM recoil kinetic energy distributions, table of observed β values, β values versus translational energy (PDF)

■ AUTHOR INFORMATION

Corresponding Author

Bradley F. Parsons − *Department of Chemistry and Biochemistry, Creighton University, Omaha, Nebraska 68178, United States;* orcid.org/0000-0002-0749-8257; Email: bparsons@creighton.edu

Authors

Adrian W. Draney − *Department of Chemistry and Biochemistry, Creighton University, Omaha, Nebraska 68178, United States*

Hunter J. Warder − *Department of Chemistry and Biochemistry, Creighton University, Omaha, Nebraska 68178, United States*

Marcos R. Rivera − *Department of Chemistry and Biochemistry, Creighton University, Omaha, Nebraska 68178, United States*

Michael K. Onder − *Department of Chemistry and Biochemistry, Creighton University, Omaha, Nebraska 68178, United States*

Complete contact information is available at:

https://doi.org/10.1021/acs.jpca.1c10514
J. Phys. Chem. A XXXX, XXX, XXX−XXX

https://pubs.acs.org/10.1021/acs.jpca.1c10514

Notes

The authors declare no competing financial interest.

■ ACKNOWLEDGMENTS

These experiments were supported by a Nebraska NASA EPSCoR Research Mini-Grant and financial assistance from the Betty and Donald J. Baumann Family Fund for Research and Outreach. We also gratefully acknowledge material assistance from the Department of Chemistry and Biochemistry at Creighton University. We thank Professor Lionel Poisson for supplying a copy of his LabView pBasex program, and we thank Professor David Szpunar at the University of Wisconsin at Stevens Point and Dr. Benj Fitzpatrick for fruitful discussions regarding these experiments.

■ REFERENCES

(1) Rollins, A. W.; Rickly, P. S.; Gao, R.-S.; Ryerson, T. B.; Brown, S. S.; Peischl, J.; Bourgeois, I. Single-Photon Laser-Induced Fluorescence Detection of Nitric Oxide at Sub-Parts-Per-Trillion Mixing Ratios. *Atmos. Meas. Tech.* **2020**, *13*, 2425−2439.

(2) Nee, J. B.; Juan, C. Y.; Hsu, J. Y.; Yang, J. C.; Chen, W. J. The Electronic Quenching Rates of NO (A $^2\Sigma^+$, v'=0-2). *Chem. Phys.* **2004**, *300*, 85−92.

(3) Guardado, J. L.; Hood, D. J.; Luong, K.; Kidwell, N. M.; Petit, A. S. Stereodynamic Control of Collision-Induced Nonadiabatic Dynamics of NO (A $^2\Sigma^+$) with H_2, N_2, and CO: Intermolecular Interactions Drive Collision Outcomes. *J. Phys. Chem. A* **2021**, *125*, 8803−8815.

(4) Lozeille, J.; Daire, S. E.; Gamblin, S. D.; Wright, T. G.; Lee, E. P. F. The A ← X (1+1) REMPI Spectrum and High-Level ab initio Calculations of the Complex Between NO and N_2. *J. Chem. Phys.* **2000**, *113*, 10952−10961.

(5) Luxford, T. F. M.; Sharples, T. R.; McKendrick, K. G.; Costen, M. L. Pair-correlated Stereodynamics for Diatom-diatom Rotational Energy Transfer: NO(A $^2\Sigma^+$) + N_2. *J. Chem. Phys.* **2017**, *147*, 013912.

(6) Mack, P.; Dyke, J. M.; Wright, T. G. Calculated Thermodynamics of Reactions Involving NO^+ X Complexes (where X = H_2O, N_2, and CO_2). *Chem. Phys.* **1997**, *218*, 243−256.

(7) Mack, P.; Dyke, J. M.; Smith, D. M.; Wright, T. G. Preliminary Report of the Observation of the A $^2\Sigma^+$ ← X $^2\Pi$ Transition in N_2 NO. *Chem. Phys. Lett.* **1998**, *284*, 423−428.

(8) Bergeron, D. E.; Musgrave, A.; Wright, T. G. (2+1) REMPI Spectroscopy of the NO-CO, NO-N_2, and NO-{N_2, Ar} van der Waals Complexes in the Region of the 4s and 3d Rydberg states. *Phys. Chem. Chem. Phys.* **2006**, *8*, 4758−4765.

(9) Wen, B.; Meyer, H.; Kłos, J. The Structure of the NO(X $^2\Pi$)-N_2 Complex: A Joint Experimental-theoretical Study. *J. Chem. Phys.* **2010**, *132*, 154305.

(10) Parsons, B. F.; Jayson, C. J.; Szpunar, D. E.; Cook, M. M. Photodissociation of the N_2-NO Complex Between 225.8 and 224.0 nm. *J. Phys. Chem. A* **2021**, *125*, 3406−3414.

(11) Sharples, T. R.; Luxford, T. F. M.; Townsend, D.; McKendrick, K. G.; Costen, M. L. Rotationally Inelastic Scattering of NO(A $^2\Sigma^+$) + Ar: Differential Cross Sections and Rotational Angular Momentum Polarization. *J. Chem. Phys.* **2015**, *143*, 204301.

(12) Mills, P. D. A.; Western, C. M.; Howard, B. J. Rotational Spectra of Rare Gas-Nitric Oxide van der Waals Molecules. 2. The Structure and Spectrum of Argon-Nitric Oxide. *J. Phys. Chem.* **1986**, *90*, 4961−4969.

(13) Holmes-Ross, H. L.; Valenti, R. J.; Yu, H.-G.; Hall, G. E.; Lawrance, W. D. Rotational and Angular Distributions of NO Products from NO-Rg (Rg = He, Ne, Ar) Complex Photodissociation. *J. Chem. Phys.* **2016**, *144*, 044309.

(14) Kłos, J.; Alexander, M. H.; Hernandez-Lamoneda, R.; Wright, T. G. Interaction of NO (A $^2\Sigma^+$) with Rare Gas Atoms: Potential Energy Surfaces and Spectroscopy. *J. Chem. Phys.* **2008**, *129*, 244303.

(15) Holmes-Ross, H. L.; Lawrance, W. D. The Dissociation of NO-Ar (A) from Around Threshold to 200 cm^{-1} Above Threshold. *J. Chem. Phys.* **2010**, *133*, 014304.

(16) Holmes-Ross, H. L.; Lawrance, W. D. The Binding Energies of NO-Rg (Rg = He, Ne, Ar) Determined by Velocity Map Imaging. *J. Chem. Phys.* **2011**, *135*, 014302.

(17) Holmes-Ross, H. L.; Lawrance, W. D. Anomalous behavior in NO-Ar (A) Photodissociation Near Threshold: A Significant Contribution from Thermally Populated States. *Chem. Phys. Lett.* **2008**, *458*, 15−18.

(18) Gordon, R. J.; Hall, G. E. Applications of Doppler Spectroscopy to Photofragmentation. *Adv. Chem. Phys.* **1996**, *96*, 1−50.

(19) Roeterdink, W. G.; Strecker, K. E.; Hayden, C. C.; Janssen, M. H. M.; Chandler, D. W. Imaging the Rotationally State-Selected NO(A,n) Product from the Predissociation of the A State of the NO-Ar van der Waals Cluster. *J. Chem. Phys.* **2009**, *130*, 134305.

(20) Parsons, B. F.; Szpunar, D. E. Investigation of O_2-X (X = Pyrrole or Pyridine) Cluster Photodissociation Near 226 nm. *J. Phys. Chem. A* **2020**, *124*, 10152−10161.

(21) Eppink, A. T. J. B.; Parker, D. H. Velocity Map Imaging of Ions and Electrons Using Electrostatic Lenses: Application in Photoelectron and Photofragment Ion Imaging of Molecular Oxygen. *Rev. Sci. Instrum.* **1997**, *68*, 3477−3484.

(22) Schneider, C. A.; Rasband, W. S.; Eliceiri, K. W. NIH Image to ImageJ: 25 Years of Image Analysis. *Nat. Methods* **2012**, *9*, 671−675.

(23) Tsuji, K.; Shibuya, K.; Obi, K. Bound-bound A $^2\Sigma^+$ - X $^2\Pi$ Transition of NO-Ar van der Waals Complexes. *J. Chem. Phys.* **1994**, *100*, 5441−5447.

(24) Garcia, G. A.; Nahon, L.; Powis, I. Two-Dimensional Charged Particle Image Inversion Using a Polar Basis Function Expansion. *Rev. Sci. Instrum.* **2004**, *75*, 4989−4996.

(25) Dribinski, V.; Ossadtchi, A.; Mandelshtam, V. A.; Reisler, H. Reconstruction of Abel-Transformable Images: The Gaussian Basis-set Expansion Abel Transform Method. *Rev. Sci. Instrum.* **2002**, *73*, 2634−2642.

(26) Pechukas, P.; Light, J. C.; Rankin, C. Statistical Theory of Chemical Kinetics. Application to Neutral-Atom-Molecule Reactions. *J. Chem. Phys.* **1966**, *44*, 794−805.

(27) North, S. W.; Hall, G. E. Quantum Phase Space Theory for the Calculation of v.j Vector Correlations. *J. Chem. Phys.* **1996**, *104*, 1864−1874.

(28) North, S. W.; Hall, G. E. Vector Scalar Correlations in Statistical Dissociation: The Photodissociation of NCCN at 193 nm. *J. Chem. Phys.* **1997**, *106*, 60−76.

(29) Klippenstein, S. J.; Cline, J. I. Classical Phase Space Theory for Product State Distributions with Application to the v-j Vector Correlation. *J. Chem. Phys.* **1995**, *103*, 5451−5460.

(30) Parsons, B. F.; Chandler, D. W.; Sklute, E. C.; Li, S. L.; Wade, E. A. Photodissociation Dynamics of Ar-NO Clusters. *J. Phys. Chem. A* **2004**, *108*, 9742−9749.

(31) Huber, K. P.; Herzberg, G. H. Constants of Diatomic Molecules. In *NIST Chemistry WebBook*; Linstrom, P. J., Mallard, W. G., Eds.; NIST Standard Reference Database Number 69; National Institute of Standards and Technology: Gaithersburg MD, 2003; p 20899.